Effect of the excitation waveform on the average power and peak power delivered by a piezoelectric generator

Kevin Nadaud, Guylaine Poulin-Vittrant, Daniel Alquier

Effect of the excitation waveform on the average power and peak power delivered by a piezoelectric generator

Kevin Nadaud[a,*], Guylaine Poulin-Vittrant[a], Daniel Alquier[a]

[a]*GREMAN UMR 7347, Université de Tours, CNRS, INSA-CVL, 16 rue Pierre et Marie Curie, 37071 Tours, France*

Abstract

The theoretical power delivered by piezoelectric generators (PG) is a key parameter for their design optimization and for the determination of the power management circuit which should be designed especially for the targeted device to be supplied. Most often, when the PG is connected to a resistive load, a maximum of average power occurs at a given load value which should be determined by sweeping the resistive load. Although the determination of this optimal load is obvious in the case of a sine signal, as it is matching the internal impedance of the PG, the cases of non-sine signals are more complex.

In this paper, we show that the waveform of the mechanical force applied to the PG significantly influences the generated power and the optimal load. We propose a method to predict the average power produced by a PG as a function of the load, even if the waveform is not a sine. The study is focused on a square waveform with variable exponential rising time, corresponding to realistic mechanical excitations, and shows that the force rising time drastically influences the mean power delivered by PGs having a capacitive internal impedance, for example some ZnO nanowires-based PGs. We also show that the peak instantaneous power, often reported as PG performance metric in literature, largely overestimates the truly available power.

Keywords: energy harvesting, piezoelectric, modeling, peak power, average power

1. Introduction

To supply the ever-increasing number of portable devices, a tendency is to build generators, in particular piezoelectric ones (PG) to harvest the wasted mechanical energy which can have various origins (ambient vibrations, human body movements).

*Corresponding author, Tel.: +33 247 366 947 ; fax: +33 247 367 121.
Email address: kevin.nadaud@univ-tours.fr (Kevin Nadaud)

In order to directly implement the lead-free directives, developments of nanomaterials such as ZnO nanowires have been investigated in PGs due their piezoelectric properties and bio-compatibility [1–5]. PGs can be used to provide the electrical energy to devices such as sensors, actuators and wireless transmitters [6–9]. An advantage of the PGs is their ability to collect the otherwise wasted mechanical energy, such as human body movements and ambient vibrations. PGs can be used to power an electronic device via a capacitor [10, 11] as temporary energy storage element and also can be used to charge a small embedded battery [12, 13].

The characterization of the generated voltage and power of a PG is generally carried out by loading the PG with a variable resistance R_L, as presented in Fig. 1. Depending on the characterization method, the voltage across the load (named $v_s(t)$) and/or the current through the load (named $i_s(t)$) are measured. This allows the determination of the short circuit current (limit at very low load value) and the open circuit voltage (limit at high load value). Moreover, according to Ohm's law, the instantaneous power delivered to a purely resistive load R_L is:

$$p(t, R_L) = \frac{(v_s(t, R_L))^2}{R_L} = (i_s(t, R_L))^2 R_L \tag{1}$$

The average power P_{ave} versus R_L can be deduced by taking the mean value over a period T:

$$P_{ave}(R_L) = \frac{1}{T} \int_{-\frac{T}{2}}^{+\frac{T}{2}} p(t, R_L)\, \mathrm{d}t \tag{2}$$

This function of R_L presents an optimal at a given load named R_L^{ave}. The knowledge of this optimal load is necessary to optimize the rectifier and conditioner circuit.

As a piezoelectric NW behaves as a charge generator, the PG is usually modeled as a current source in parallel with a lossy capacitor, or by an equivalent Thevenin generator consisting of a controlled voltage source (corresponding to the open circuit voltage and noted $v_{OC}(t)$) in series with an internal impedance called Z_{PG} as shown in Fig. 1.

The magnitude and the shape of the voltage source depends on the applied force. In the case of PG submitted to a quasi-static force, $v_{OC}(t)$ is proportional to the applied force [14–16]. As a consequence, the temporal waveform of the applied force is similar to the open circuit waveform. Even if some papers mention the applied waveform, only few have studied the influence of a non sine excitation waveform on the generated power [14, 17]. This paper studies the case of periodic waveforms contrary to impulsive waveforms already studied in literature [18, 19].

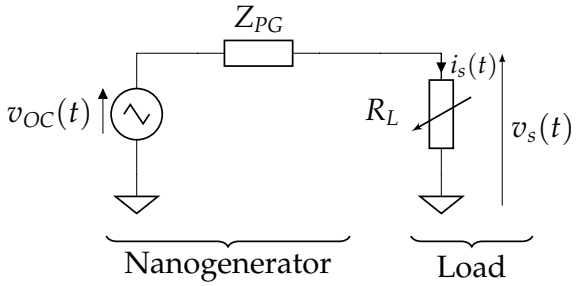

Figure 1: Common electrical circuit used for functional characterization of PGs.

In the case of a uniform active material, such as a bulk piezoelectric ceramic, the open circuit voltage and the internal impedance of the generator can be determined using the geometry of the generator (thickness, surface) and intrinsic properties of the material (dielectric permittivity, piezoelectric coefficient, Young modulus...). In the case of a nano-material based generator, the device is usually a composite comprising the active material (which produces the charges) and a matrix (which ensures the robustness of the device and/or acts as a capacitive layer), in that case the determination of the circuit parameters has to be done using numerical simulations [15, 20–22]. For any type of generator, the open circuit voltage can be obtained by measuring the output of the generator at high resistive load and the internal impedance using conventional impedance spectroscopy as it is explained later on.

In this paper, we show that the open circuit voltage waveform (proportional to the applied force when the PG is in quasi-statique regime) largely influences the PG characteristics of average power and peak power versus resistive load. We also propose a method to predict the average power by knowing the waveform of the open circuit voltage and the internal impedance of the considered PG. The first part is devoted to provide a quick review of theoretical calculation of the average power calculation at the output of a two-port network. Then, the derived expression is applied to the case of a PG with a capacitive internal impedance, corresponding to a PG with a low electromechanical coupling coefficient. To confirm the obtained results, a practical study is carried out using lumped capacitor and a low frequency signal generator. Finally, the functional characterization of piezoelectric buzzer, used as a PG, is made for different waveforms of the applied force. We show the harmonics contained into a signal not only increase the average and peak powers, which seems natural since harmonics contain energy, but also the optimal load range of the PG is modified by these harmonics.

The waveforms considered in this paper are common waveforms, such as the sine

function which is the base of every harmonic analysis, and also the triangle, sawtooth and square functions. We mostly focus on the square one, since this signal is similar to an impact and thus corresponds more to realistic cases of excitation. In order to take into account the rising time, an additional waveform, which consists of a square waveform with exponential rise and fall, simply called "exponential signal", is also studied.

2. Theoretical study

If we consider a two-port network, sometimes called quadripole, presented in Fig. 2, having a transfer function expressed as:

$$\underline{H}(j\omega, R_L) = \frac{\underline{V_s}(j\omega)}{\underline{V_e}(j\omega)} \tag{3}$$

The dependence of $\underline{V_s}(j\omega)$ with the load resistance R_L is implicit, since the transfer function generally depends on the load value, due to its output impedance. This dependence is explicitly noted in $\underline{H}$ to remind this fact. The transfer function can be decomposed into magnitude G and phase ϕ:

$$G(\omega, R_L) = |\underline{H}(j\omega, R_L)|, \qquad \phi(\omega, R_L) = \arg\left[\underline{H}(j\omega, R_L)\right] \tag{4}$$

This transfer function is only valid when the input signal is monochromatic and allows us to obtain the temporal expression of the output for a given input. Firstly, we consider an input signal with the temporal expression:

$$v_e(t) = V_e \sin\left(\omega_0 t + \phi_e\right) \tag{5}$$

where $\omega_0 = 2\pi f_0$ is the angular frequency of the signal, V_e the magnitude and ϕ_e the initial phase. The temporal expression of the output signal can thus be obtained:

$$v_s(t, R_L) = V_e G(\omega_0, R_L) \sin\left(\omega_0 t + \phi_e + \phi(\omega_0, R_L)\right) \tag{6}$$

If we consider the case of an input signal which is not monochromatic but still periodic, this input signal can be decomposed into a time series (Fourier series development):

$$v_e(t) = a_0 + \sum_{n=1}^{+\infty} a_n \cos\left(n\omega_0 t\right) + b_n \sin\left(n\omega_0 t\right) \tag{7}$$

The output signal can also be deduced from (3) which must be applied to each harmonic, by considering the modulus and the phase of the transfer function at the $n\omega_0$

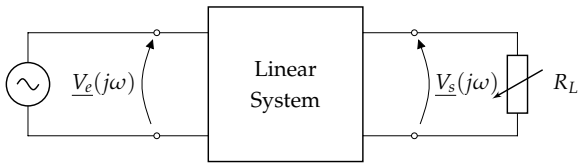

Figure 2: A generic quadripole fed by an ideal voltage source and loaded by a resistor R_L.

angular frequency:

$$v_s(t, R_L) = a_0 G(0, R_L) + \sum_{n=1}^{+\infty} G(n\omega_0, R_L)\left(a_n \cos\left(n\omega_0 t + \phi(n\omega_0)\right) + b_n \sin\left(n\omega_0 t + \phi(n\omega_0)\right)\right) \quad (8)$$

With the output signal expression, it is possible to calculate the average power $P_{ave}(R_L)$ dissipated into the load R_L during the period T:

$$P_{ave}(R_L) = \frac{1}{T}\int_{-\frac{T}{2}}^{+\frac{T}{2}} \frac{\left(v_s(t, R_L)\right)^2}{R_L}\,\mathrm{d}t \quad (9)$$

Using the Parseval's theorem, the following expression of the average power can be deduced:

$$P_{ave}(R_L) = \frac{\left(a_0 G(0, R_L)\right)^2}{R_L} + \frac{1}{2}\left(\sum_{n=1}^{+\infty} \frac{G^2(n\omega_0, R_L)}{R_L}\left(a_n^2 + b_n^2\right)\right) \quad (10)$$

One can note that only the magnitude of the transfer function is used for the mean power computation where the phase of the transfer function does not appear. As a conclusion, the full $P_{ave}(R_L)$ curve corresponds to the sum of each $(G(n\omega_0, R_L))^2/R_L$ curve weighted by $a_n^2 + b_n^2$ factor. Each $(G(n\omega_0, R_L))^2/R_L$ curve may present an optimal point versus R_L and the full $P_{ave}(R_L)$ curve optimal will depend on the weighting applied to each frequency. In the whole manuscript, the word *computation* refers to the power calculated using (10).

3. Application to a PG with capacitive internal impedance

The study detailed in this part is the case of a PG having a capacitive internal impedance such as a nanowire-polymer composite generator with a vertical configuration [2, 16, 23, 24] or lateral configuration [25, 26]. We consider first a lossless capacitive impedance (which means that the dielectric losses angle $\tan\delta$ is null), but the formula can be applied to any type of lossy capacitive and/or $p-n$ junction generator [27, 28].

The equivalent circuit for the PG connected to the load is presented in Fig. 3. In the case of a series resistance, the transfer function can be simply obtained using:

$$\underline{H}(j\omega, R_L) = \frac{V_s(j\omega)}{V_e(j\omega)} = \frac{R_L}{R_L + \underline{Z_{PG}}(j\omega)} \quad (11)$$

In the present case (lossless capacitive internal impedance), the transfer function magnitude (3) can be explicitly derived:

$$G(\omega, R_L) = \frac{R_L}{\sqrt{R_L^2 + \left(\frac{1}{C_{PG}\omega}\right)^2}} \tag{12}$$

Where C_{PG} represents the internal capacitance of the PG. In the case of a monochromatic signal at an angular frequency ω_0, the optimal load can be calculated using:

$$R_L^{ave} = \frac{1}{C_{PG}\omega_0} \tag{13}$$

In the case of a signal containing harmonics, for the n^{th} harmonic, the optimal load is:

$$R_{L,n}^{ave} = \frac{1}{C_{PG}n\omega_0} = \frac{R_{L,1}^{ave}}{n} \tag{14}$$

Consequently, each harmonic contained in $v_{OC}(t)$ signal has a different optimal load in the case of a capacitive internal impedance. The maximum power with respect to the load, for the n^{th} harmonic, is:

$$P_{ave}(n\omega_0, R_{L,n}^{ave}) = \frac{(a_n^2 + b_n^2)}{R_{L,n}^{ave}} G^2(n\omega_0, R_{L,n}^{ave}) = \frac{n(a_n^2 + b_n^2)}{2R_{L,1}^{ave}} \tag{15}$$

a_n and b_n are the Fourier coefficients of the open circuit voltage (7). One can note the factor n within equation which means, even if the a_n and b_n coefficients decrease when n increases, the harmonics are enhanced by the capacitive internal impedance.

For the experimental study, we considered an internal capacitance of 10 nF and the resistive load was varied from 10 kΩ to 100 MΩ corresponding to the available load range for our test bench. This value of the internal impedance has been chosen because the studied generators have a capacitive internal impedance in that range of magnitude. The value of the internal impedance does not change the results obtained is that study, a sensitivity analysis is presented later in the manuscript. The chosen fundamental frequency is 5 Hz since most of our PG characterization campaigns are made at this frequency [23, 29]. The model derived in this paper works even if the fundamental frequency is modified, provided that we stay in the quasi-static regime or at least far away from resonance modes.

In order to validate the theoretical calculation of the average power delivered by the PG, the following experiment has been carried out: an Agilent 33250 signal generator ($v_{OC}(t)$) in series with a 10 nF capacitor (C_{PG}) were used to emulate the capacitive PG, which was connected to a variable resistance, as on Fig. 3. The acquisition of the waveform has been made using an Agilent DSO5054A oscilloscope.

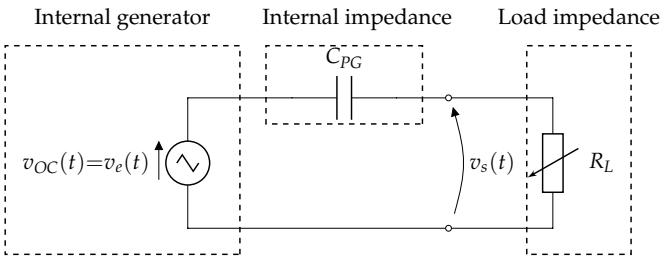

Figure 3: Equivalent circuit of the PG presenting a capacitive impedance, and connected to a resistive load for the experimental tests.

3.1. Influence of the waveform of the mechanical force applied to the PG

The previously derived expressions are used here to determine the influence of the waveform on the generated power and the optimal load for a PG with capacitive impedance. Each harmonic presents an optimal load (since the optimal load of a monochromatic signal depends on the frequency (13)) and the effective optimal load (maximizing the total average power) thus depends on the weight of all harmonics. As open circuit voltage $v_{OC}(t)$ in Fig. 3, four different waveforms are studied here: sine, sawtooth, square and triangle. The expression of the sine signal with magnitude V_{OC} is:

$$v_{sine}(t) = V_{OC} \sin(\omega_0 t) \tag{16}$$

The Fourier series development of the sawtooth signal with magnitude V_{OC} is:

$$v_{saw}(t) = \frac{2V_{OC}}{\pi} \sum_{n=1}^{+\infty} (-1)^n \frac{\sin(n\omega_0 t)}{n} \tag{17}$$

The Fourier series development of the square signal with magnitude V_{OC} is:

$$v_{squ}(t) = \frac{4V_{OC}}{\pi} \sum_{k=0}^{+\infty} \frac{\sin((2k+1)\omega_0 t)}{2k+1} \tag{18}$$

The Fourier series development of the triangle signal with magnitude V_{OC} is:

$$v_{tri}(t) = \frac{8V_{OC}}{\pi^2} \sum_{k=0}^{+\infty} (-1)^k \frac{\sin((2k+1)\omega_0 t)}{(2k+1)^2} \tag{19}$$

The resulting optimal load is quite difficult to obtain analytically, nevertheless, it depends on the harmonic content of the input signal. For the computation of the $P_{ave}(R_L)$ curve, based on (10) and (12) 10^4 harmonics are considered. This number will be justified later on in § 3.2.

Fig. 4 represents the computed and measured mean powers as a function of the load R_L for different waveforms with the same magnitude. One can note the very good agreement between computation and measurement, showing the efficiency of

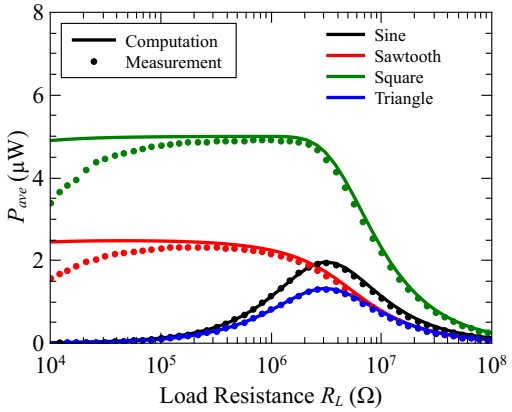

Figure 4: Computed (lines) and measured (bullets) mean power supplied to the load as a function of the load R_L for different waveforms.

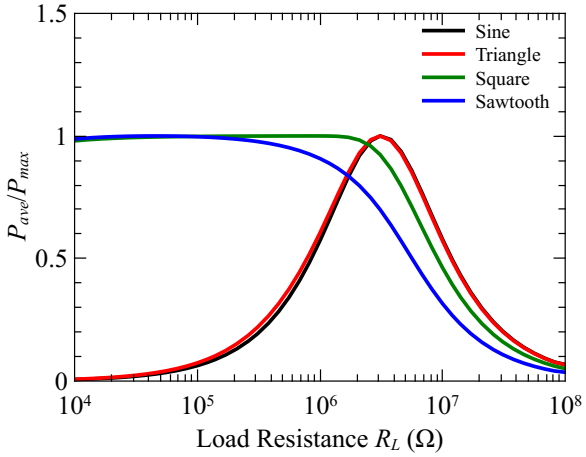

Figure 5: Normalized computed mean power according to the max value as a function of the load R_L for different waveforms.

the model to predict the average power for a given generic waveform. For the sine waveform, the optimal load is very close to the theoretical value of $R_L^{ave} = 3.18\,\mathrm{M\Omega}$, (13). The optimal load value is lower for the sawtooth signal than for the square signal which is itself showing lower optimal load than the sine signal. This comes from the fact that for the square signal there are only odd harmonics, whereas the sawtooth signal contains both odd and even harmonics, leading to a higher shift of the optimal load. As a consequence, the calculation of the optimal load using (13) is not valid for sawtooth and square signals, due to the presence of harmonics.

The power at optimal load is higher for the square and the sawtooth signals than for the sine wave. This is due to the harmonics, enhanced by the capacitive impedance effect, and all these harmonics contribute to the total average power. For the triangle signal, only a very small shift of the curve towards lower loads is visible and the maximum power is 35 % lower than for the sine waveform. The very small shift can be explained by the fact that the harmonics weighting coefficient is proportional to n^{-2}

Table 1: Summary of the computed and measured range of optimal load and power at optimal load for different waveforms.

	Computation		Measurement	
Waveform	Range of optimal load	Maximum power P_{ave}^{max}	Range of optimal load	Maximum power P_{ave}^{max}
Sine	2.0 MΩ to 5.1 MΩ	2 µW	1.9 MΩ to 4.8 MΩ	2 µW
Triangle	1.9 MΩ to 5.0 MΩ	1.3 µW	1.9 MΩ to 4.7 MΩ	1.3 µW
Sawtooth	10 kΩ to 1.1 MΩ	2.5 µW	31 kΩ to 1.3 MΩ	2.3 µW
Square	10 kΩ to 3.3 MΩ	5 µW	29 kΩ to 3.1 MΩ	4.9 µW

(with n the harmonic order), whereas for sawtooth and square signals the harmonics weighting coefficient is proportional to n^{-1}. As a consequence, the contribution of harmonics to the total power becomes fastly negligible. In the case of a triangle with the same magnitude as a sine, a $8/\pi^2$ coefficient is present on the fundamental according to the Fourier series decomposition (19). Since the contribution of the other harmonics to the average power is almost negligible, the maximum value of the average power is lower for this triangle waveform compared to the sine one.

One can note that the harmonics content largely changes the shape of the $P_{ave}(R_L)$ curve as shown on Fig. 5. For sawtooth and square signals, the power is close to the maximum value on a wide range of load, here three orders of magnitude and even 6 orders of magnitude, according to [14] which proposes a Finite Element Modelling study performed on a PZT ceramic submitted to a vertical force. The main consequence is that the equivalent load of the circuit connected to the PG seems to be less critical when the mechanical excitation contains harmonics. In order to better show the effect of the waveform on the shape of the $P_{ave}(R_L)$ curve, let us calculate the range of resistance over which the power exceeds 90 % of the maximum value. The results are summarized in table 1. For the sine and triangle waveforms, the measured ranges are very similar to the ones obtained in simulation. For the sawtooth and square waveforms, the upper limit of the range is well predicted, and there is only a small difference on the lower limit.

The small difference between the measured and the computed powers at small loads, for the square and sawtooth signals, is attributed to the rising time which is not null for a voltage provided by a signal generator. Ideal square or sawtooth are not physical signals, since they present discontinuities, and for this reason, in § 3.3 we propose a signal which is more physical with a non-null rising time, whose effect on the $P_{ave}(R_L)$ curve will be presented.

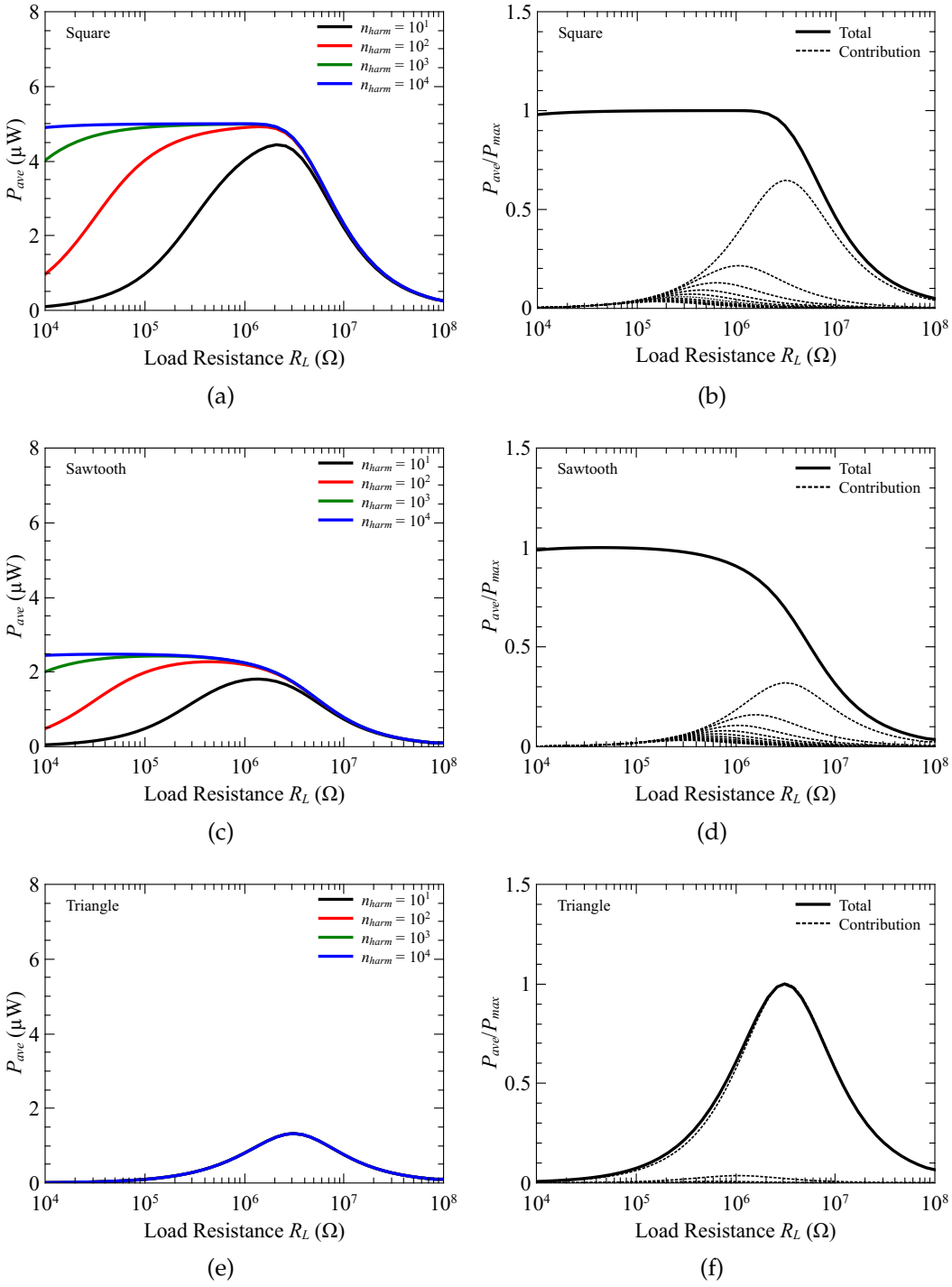

Figure 6: Mean power as a function of the load R_L for increasing number of harmonics used for the computation, when V_{OC} is a square signal (a), a sawtooth signal (c) or a triangle signal (e). Decomposition (dashed line) and total (full line) power as a function of the load R_L, when V_{OC} is a square signal (b), a sawtooth signal (d) or a triangle signal (f).

3.2. Influence of the number of harmonics used to compute the average power

The three considered signals are described as an infinite sum, that must therefore be truncated for the computation. Fig. 6(a) shows the effect of the number of considered harmonics on the average power delivered to the load, for the square waveform. One can note that, when the number of considered harmonic increases, the maximum value of power increases (and becomes stable after 10^3 harmonics) and the shape of the curve is greatly modified, showing a clear increase of the bandwidth with respect to the load resistance. A similar effect is visible for the sawtooth signal (Fig. 6(c)) but this effect is not present for the triangle signal (Fig. 6(e)) because the decrease of the harmonics magnitude is faster (n^{-2} instead of n^{-1}). This shows that if the V_{OC} harmonics magnitude follows a n^{-2} law, these harmonics (other than the fundamental) almost do not contribute to the power. On the contrary, if the V_{OC} harmonics magnitude follows a n^{-1} law, these harmonics contribute significantly to the power. As a consequence, it is crucial to take into account a sufficient number of harmonics when the harmonics of the mechanical excitation decrease proportionally to n^{-1}.

To better understand this point, it important to notice that, as the decrease of the V_{OC} harmonics magnitude of the harmonics is proportional to n^{-1} (case of sawtooth (17) and square (18) signals) the power of each harmonic is proportional to n^{-2}. Nevertheless due to the capacitive effect, the high frequency harmonics are enhanced. This effect is illustrated in Fig. 6(b) which presents the contribution of each harmonic into the total power. One can note the magnitude of the harmonics is lower than the fondamental contribution but not negligible. The maximum value of the harmonics contribution is proportional to n^{-1} according eq. (15). For the triangle signal, since the harmonics magnitude is proportional to n^{-2} the power component of each harmonic is proportional to n^{-4} and thus the contribution of harmonics becomes quickly negligible since the maximum value of each harmonic is proportional to n^{-3} as illustrated in Fig. 6(f). Finally, we can notice that the important parameter is the polynomial law followed by the coefficients of the Fourier series decomposition of the considered V_{OC} signal.

In practice, the signal is not purely square and there are rising and falling times. In the next parts, the case of physical signals will be studied such as a square signal with an exponential rising.

3.3. Physical signals

In this section, we consider more realistic open circuit voltage signals, hence corresponding to more realistic mechanical excitations applied to the PG, since square and sawtooth signals both present discontinuities which are not physical. Instead of the square, hereafter we propose a square, with rise and fall times represented by an exponential function with a time constant τ, as presented Fig. 7(a). For simplicity, this periodic signal is simply called "exponential signal". A small value of τ, compared to the period T of the signal, represents a fast system, and hence the signal shape is very close to the square one. On the other hand, a high value of τ represents a slow system and, thus, the obtained signal which is quite far from the original square.

To obtain the Fourier series decomposition of the exponential signal, it is possible to use the Fourier series of the square (18) and to apply a first-order low-pass filter with a time constant τ. Similarly to the square waveform, even Fourier coefficients are null and the odd ones are :

$$a_n^{exp} = -\frac{4V_{OC}}{\pi}\frac{\omega_0\tau}{1+(n\omega_0\tau)^2} \qquad \text{and} \qquad b_n^{exp} = \frac{4V_{OC}}{\pi n}\frac{1}{1+(n\omega_0\tau)^2} \tag{20}$$

The full demonstration is presented into the supplementary material.

Depending on the value of τ, the harmonic content of the signal differs. Fig. 7(b) shows the harmonic content of the exponential signal for different values of τ. For $\tau/T = 5\times10^{-5}$, a straight line is obtained. This corresponds well to harmonic coefficients following a n^{-1} law, which is the case of the original square signal. When τ increases, a second straight line appears with a 2 times higher slope, corresponding to a n^{-2} law. Higher is τ, lower is the harmonic number n at which the change of slope occurs. As a consequence, the harmonics at frequencies higher than $\frac{1}{2\pi\tau}$ contribute slightly to the power delivered by the PG to the resistive load.

The average power for an exponential waveform can be calculated using (10) by replacing the transfer function magnitude $G(\omega, R_L)$ (12) and the a_n and b_n coefficients (20):

$$P_{ave}(R_L,\omega_0,\tau) = \left(\frac{4V_{OC}}{\pi}\right)^2 \sum_{k=0}^{+\infty} \frac{R_L}{R_L^2 + \left(\frac{1}{(2k+1)C\omega_0}\right)^2} \frac{1}{(2k+1)^2\left(1+((2k+1)\omega_0\tau)^2\right)} \tag{21}$$

Fig. 8 shows the measured and theoretical mean powers as a function of the load for the exponential waveform. For small values of τ, the power curve is very flat, similarly to the curve obtained with the square waveform (Fig. 4) showing that a high

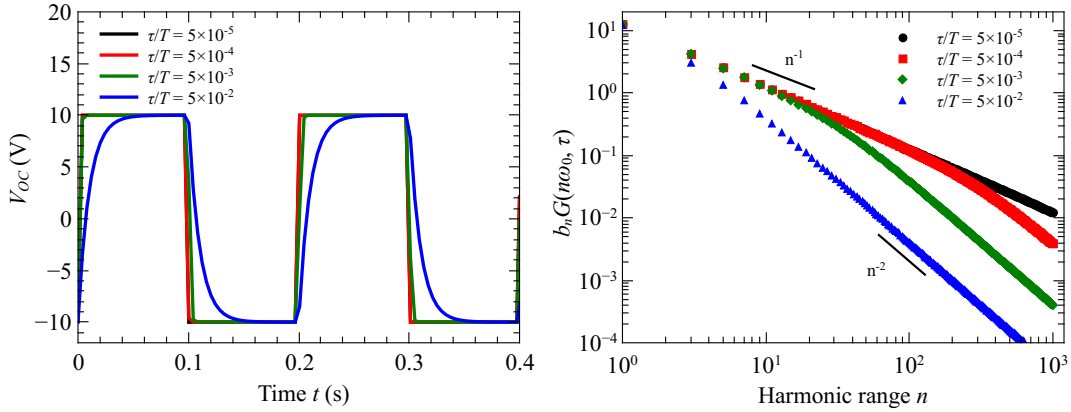

Figure 7: Waveform of the periodic exponential signal (a) and the corresponding harmonic content (b) for different values of τ/T. Only odd coefficients are represented since even coefficients are null.

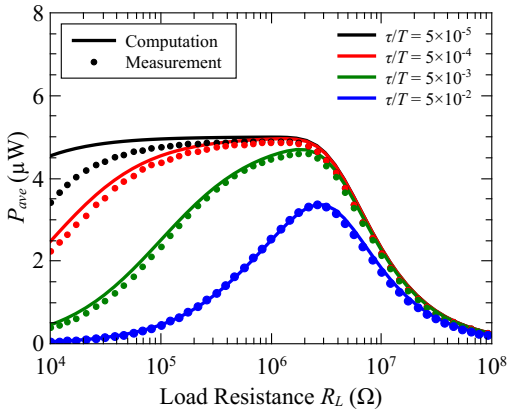

Figure 8: Measured (bullets) and computed (lines) power as a function of the load, for the periodic exponential signal having different values of τ/T.

number of harmonics contribute to the power. When τ increases, the maximum of power decreases and the curve approach the power curve obtained with a triangular or sine signal indicating that in this case the harmonics do not contribute significantly to the overall power. This clearly shows that, if the applied force presents very sharp transitions (low value of τ), the high number of harmonics contribute significantly to the harvested power. On the other hand, when the signal evolves slowly (high value of τ), the harmonics don't contribute significantly to the harvested power and the shape of the $P_{ave}(R_L)$ curve is very similar to the case of a monochromatic excitation.

The small difference between the measured and the computed powers at small loads, especially for $\tau/T = 5 \times 10^{-5}$, is attributed to the rising time which not as small as expected, similarly to what have been obtained for the square and sawtooth signals in the previous part.

A similar study concerning the non-null rising time has been done for the sawtooth

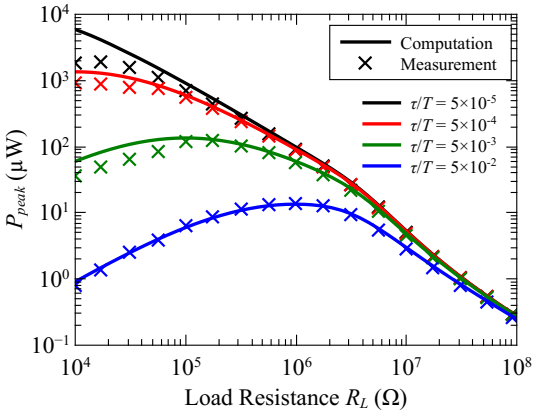

Figure 9: Measured (cross) and computed (lines) peak instantaneous powers for different values of τ/T, for an exponential waveform.

signal and is detailed into the supplementary material.

3.4. Comparison between peak and average powers delivered by a PG, for an exponential waveform.

In most of literature, presenting mechanical energy harvesters performances, only the peak instantaneous power is provided [1, 3, 4, 28] instead of the average power [27]. For an arbitrary mechanical excitation applied to the PG, leading to an arbitrary open circuit voltage, the peak instantaneous power computation is almost impossible since it relies on the time derivation of (8) which contains an infinite number of terms. In the present case, the considered equivalent circuit is sufficiently simple to compute the temporal expression by solving the associated differential equation. Of course, in more complex cases (arbitrary internal impedance of the PG), the differential equation becomes too complicated to be solved and the Fourier analysis is more convenient, even if there is an infinite sum.

For $t \in \left[0, \frac{T}{2}\right]$, the voltage across the resistor is:

$$v(t) = \begin{cases} \dfrac{2V_{OC}}{1-\frac{\tau}{R_L C_{PG}}} \left(\dfrac{\exp\left(-\frac{t}{R_L C_{PG}}\right)}{1+\exp\left(-\frac{T}{2R_L C_{PG}}\right)} - \dfrac{\exp\left(-\frac{t}{\tau}\right)}{1+\exp\left(-\frac{T}{2\tau}\right)} \right) & \text{if } \tau \neq R_L C_{PG}, \\ \dfrac{2V_{OC}}{\tau\left(1+\exp\left(-\frac{T}{2\tau}\right)\right)} \left(t - \dfrac{T\exp\left(-\frac{T}{2\tau}\right)}{2\left(1+\exp\left(-\frac{T}{2\tau}\right)\right)} \right) \exp\left(-\dfrac{t}{\tau}\right) & \text{if } \tau = R_L C_{PG} \end{cases} \tag{22}$$

See supplementary material for the complete demonstration.

Fig. 9 shows the peak instantaneous power curves as a function of the load, for different values of τ/T. These curves present very different shapes and levels compared to the average power curves plotted in the same conditions (Fig. 8). Table 2 summa-

Table 2: Summary of the optimal load range values maximizing mean power and peak power, and the corresponding power levels for different values of τ/T.

	Average power		Peak power	
τ/T	Optimal load R_L^{ave}	Maximum power P_{ave}^{max}	Optimal load R_L^{peak}	Maximum power P_{peak}^{max}
5×10^{-2}	2.6 MΩ	3.4 µW	1 MΩ	14 µW
5×10^{-3}	1.81 MΩ	4.6 µW	150 kΩ	127 µW
5×10^{-4}	1 MΩ	4.9 µW	38 kΩ	794 µW
5×10^{-5}	1 MΩ	4.9 µW	14 kΩ	1.9 mW

rizes the optimal load values R_L^{ave} and R_L^{peak}, maximizing average power and peak instantaneous power respectively. As noticed previously, when τ/T decreases, the mean power at optimal load value seems to tend to a limit, as well as the optimal load value remains constant (almost no difference between $\tau/T = 5 \times 10^{-4}$ and $\tau/T = 5 \times 10^{-5}$). For the peak instantaneous power value, the variation between $\tau/T = 5 \times 10^{-2}$ and $\tau/T = 5 \times 10^{-5}$ leads to an increase of more than two orders of magnitude on the peak value (a factor 135) and a reduction of a factor 70 of the optimal load (R_L^{peak}). This clearly shows that the peak instantaneous power is considerably influenced by the harmonics content of the mechanical excitation. This may explain the large values of peak power obtained in some papers when the excitation is very brief and intense [1, 23].

3.5. *Sensitivity analysis*

When measuring the internal impedance or the open circuit voltage of a PG, this may lead to uncertainty on the predicted average and peak powers. Since the number of parameters is quite small, a basic sensitivity analysis is presented here. In the case of a large number of parameters, it is possible to use the method presented in [30].

For a purely sine waveform, the mean power can be computed using (10) which can be explicitly derived:

$$P_{ave}(R_L, \omega_0) = V_{OC}^2 \frac{R_L}{R_L^2 + \left(\frac{1}{C_{PG}\omega_0}\right)^2} \tag{23}$$

The optimal load can be computed using (13) and the maximum average power at this optimal load is thus:

$$P_{ave}(R_L^{ave}, \omega_0) = \frac{V_{OC}^2 \omega_0 C_{PG}}{2} \tag{24}$$

Considering uncertainty on the capacitance value, the relative uncertainty on the maximum average power at this optimal load and on the optimal load are thus:

$$\left(\frac{\Delta R_L^{ave}}{R_L^{ave}}\right)_{V_{OC}} = -\frac{\Delta C_{PG}}{C_{PG}} \qquad \text{and} \qquad \left(\frac{\Delta P_{ave}}{P_{ave}}\right)_{V_{OC}} = \frac{\Delta C_{PG}}{C_{PG}} \tag{25}$$

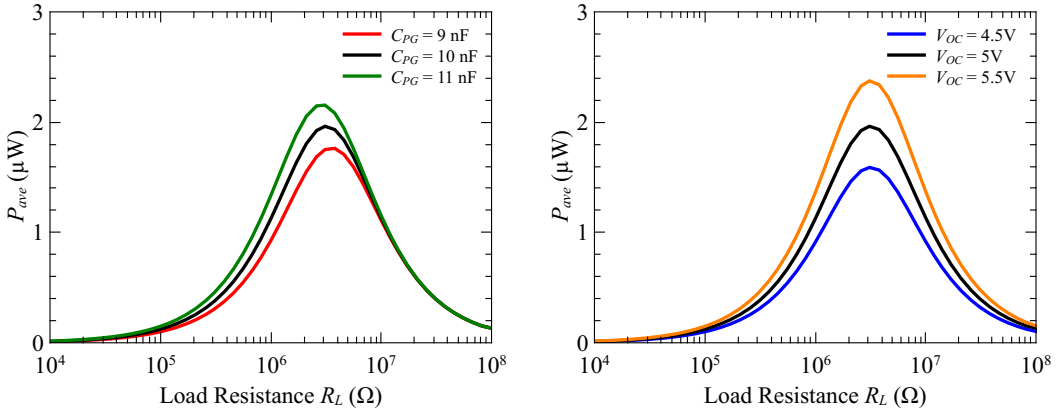

Figure 10: Computed average power as a function of the load R_L, for different values of the internal capacitance (a) and different values of the open circuit voltage (b).

This signifies that a decrease of the internal capacitance implies an increase of the optimal load and a decrease of the maximum average power. This phenomena is illustrated by Fig. 10(a).

Considering uncertainty on the open circuit voltage value, the relative uncertainty on the maximum average power at this optimal load and on the optimal load are thus:

$$\left(\frac{\Delta R_L^{ave}}{R_L^{ave}}\right)_{C_{PG}} = 0 \qquad \text{and} \qquad \left(\frac{\Delta P_{ave}}{P_{ave}}\right)_{C_{PG}} = 2\frac{\Delta V_{OC}}{V_{OC}} \tag{26}$$

This signifies that a decrease of the open circuit voltage implies no variation of the optimal load and a decrease of the maximum average power. This phenomena is illustrated by Fig. 10(b). One can note the variation of the maximum average power is larger for open circuit voltage variation than for the internal capacitance variation which comes from the square applied on the voltage in (24).

For an exponential waveform, the value of the optimal load is not straightforward to obtain analytically, thus simulation have been made in order to verify the trend described above for a sine waveform. Fig. 11(a) shows the computed average power as a function of the load R_L, for different values of the internal capacitance. For the exponential waveform, the internal capacitance influences the maximum value of the average power, similarly to what is obtained for the sine waveform. The shift of maximum power range is also visible (Fig. 11(b)). Concerning, the sensitivity to the open circuit voltage, only the maximum average power changes and the optimal load range is not affected (Fig. 12). One can note, that the shape of the $P_{ave}(R_L)$ curve is the same for any variation of both the internal capacitance or the open circuit voltage.

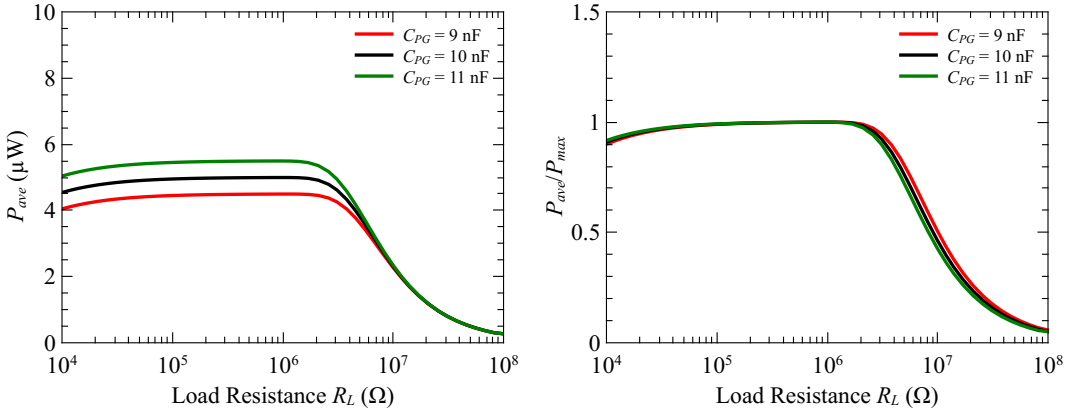

Figure 11: Computed average power (a) and normalized computed mean power according to the max value (b) as a function of the load R_L, for different values of the internal capacitance for a exponential waveform with a $\tau/T = 5 \times 10^{-5}$.

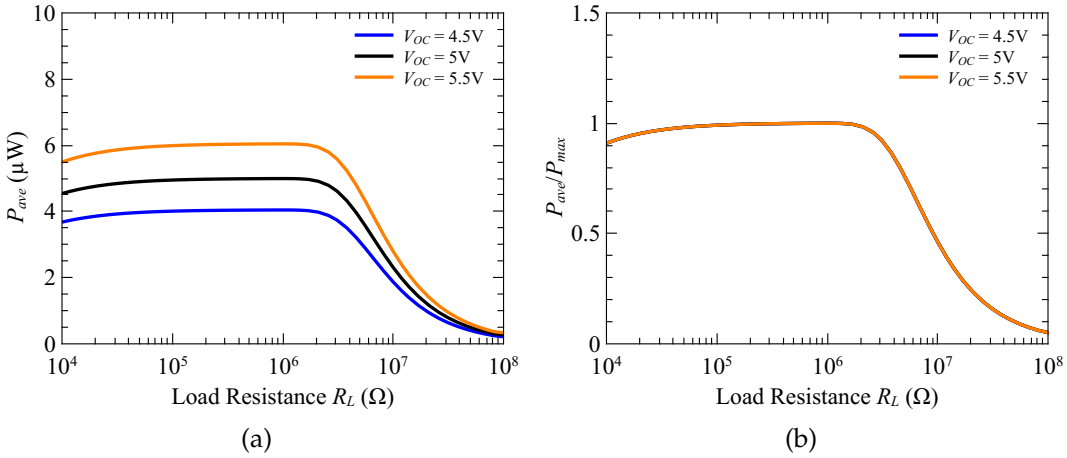

Figure 12: Computed average power (a) and normalized computed mean power according to the max value (b) as a function of the load R_L, for different values of the open circuit voltage for a exponential waveform with a $\tau/T = 5 \times 10^{-5}$.

4. Experimental validation of the power calculation

The experimental validation has been carried out using a multilayer piezoceramic plate (Noliac reference NAC2015 [31]) as actuator and a piezoelectric buzzer as PG. The NCA2015 actuator has been chosen for its high resonance frequency ($>$ 486 kHz), as a consequence, it will act in quasi-static regime at low frequency (5 Hz) and it will apply the force even to the buzzer for very sharp transitions (close to a square waveform). The actuator and the buzzer are fixed using a small screw as presented in Fig. 13. The actuator is driven using an Agilent 33250 signal generator. At the output of the buzzer, a variable resistance is connected in order to sweep the resistive load. The acquisition of the waveform has been made using an Agilent DSO5054A oscilloscope and a double buffer circuit[29] is used in order to have a high input impedance.

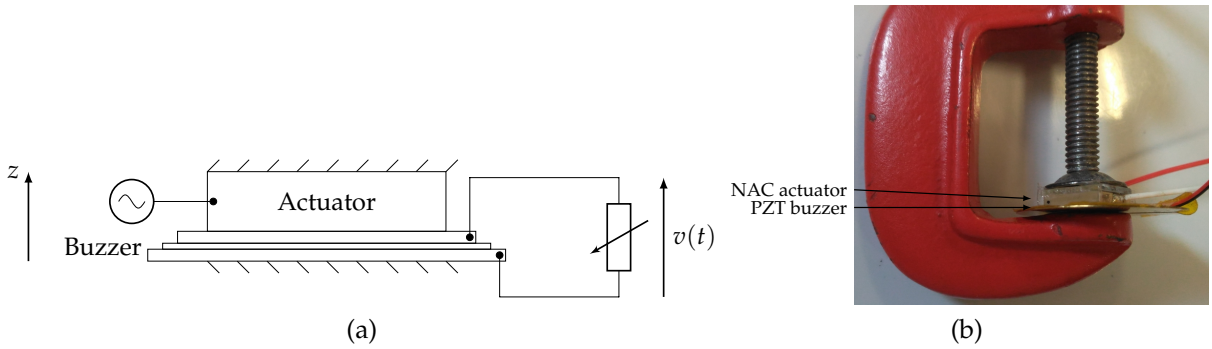

Figure 13: Schematic (a) and optical view (b) of the experimental test bench using a piezoelectric actuator and a piezoelectric buzzer (the PG). The actuator and the buzzer are fixed together using a small screw. The force is applied across the z-axis.

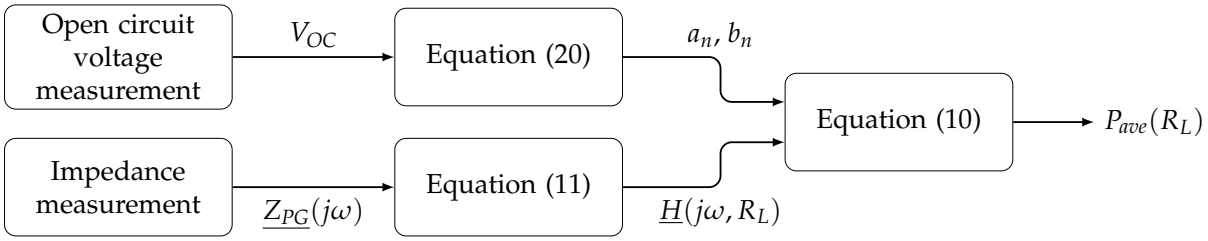

Figure 14: Workflow used to compute the average power as a function of the resistive load using the open circuit measurement and the impedance measurement.

The prediction of the average output power using (10) requires two elements, (i) the transfer function magnitude representing the loaded piezoelectric generator (11) and (ii) the Fourier series decomposition of the open circuit voltage (7). The flow chart of the calculation procedure for the assessment of the average power as a function of the resistive load and for a given waveform is shown Fig. 14.

For step (i), the transfer function (11) of the considered piezoelectric generator can be obtained by measuring the internal impedance. For step (ii), the open circuit voltage Fourier series decomposition requires the experimental determination of the V_{OC} magnitude to compute a_n and b_n using (20). This magnitude is measured in harmonic regime at low frequency (5 Hz) thanks to the double buffer circuit previously introduced.

In the 1 Hz–100 Hz frequency range, the impedance measurement has been carried out by measuring the alternative current (AC) across the buzzer, using a Keithley 6517A electrometer, while applying an AC voltage. In the 40 Hz–10 kHz frequency range, the impedance measurement has been made using Agilent 4294A impedance analyzer. The impedance magnitude and phase are shown on Fig 15(a) and the associated capacitance and loss factor, on Fig 15(b). For frequencies below 1.5 kHz, the buzzer exhibits a capacitive behavior. Resonances are visible at 2.03 kHz, 3.46 kHz,

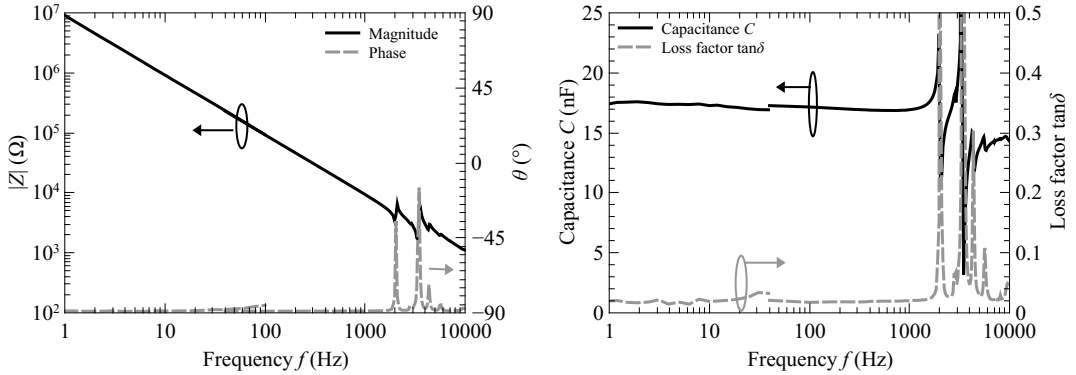

Figure 15: Magnitude and phase of the impedance (a) and associated capacitance and loss factor (b) of the piezoelectric buzzer as a function of frequency.

4.36 kHz and 5.64 kHz. For an harmonic excitation, the internal impedance of the PG corresponds to the optimal value of the load, maximizing the delivered power. According to (13), the theoretical optimal resistive load at 5 Hz is 1.9 MΩ for the considered buzzer.

For, the harmonic excitation, the optimal load corresponds well to the predicted value. For the exponential waveform with high values of τ/T ($\geq 5 \times 10^{-3}$) and for the sine waveform (Fig. 16(a)), the shape of the $P_{ave}(R_L)$ curve is accurately predicted. For the exponential waveform with small values of τ/T ($\leq 5 \times 10^{-4}$) and for the square waveform (Fig. 16(b)), a discrepancy is present at small load values. It can be attributed to the resonance modes of the piezoelectric buzzer. Nevertheless, the model predicts that the maximum average power increases when τ/T decreases and that the bandwidth with respect to the load is widened. At $\tau/T < 5 \times 10^{-4}$, the increase of average power at very small load value (inferior to $10^5\,\Omega$) is attributed to the resonance modes of the buzzer. The Fig 17(a) shows the measured and computed waveforms for $\tau/T = 5 \times 10^{-5}$ and $R_L = 100\,\text{k}\Omega$. The measured curve exhibits oscillations due to resonance modes into the material whereas these oscillations are not present on computation curve showing the limit of the quasi-static approach. This explains the difference between computed and measured powers. These differences are not visible for high values of τ/T as shown on Fig. 17(b) since oscillations (due to resonance modes) are not visible. For a better accuracy the resonance modes of the buzzer could be taken into account in the analytical model, for example using the Mason model [32].

Fig. 16(c) shows the peak instantaneous power measured for the different waveforms. With the exponential waveform, the maximum of peak power increases when

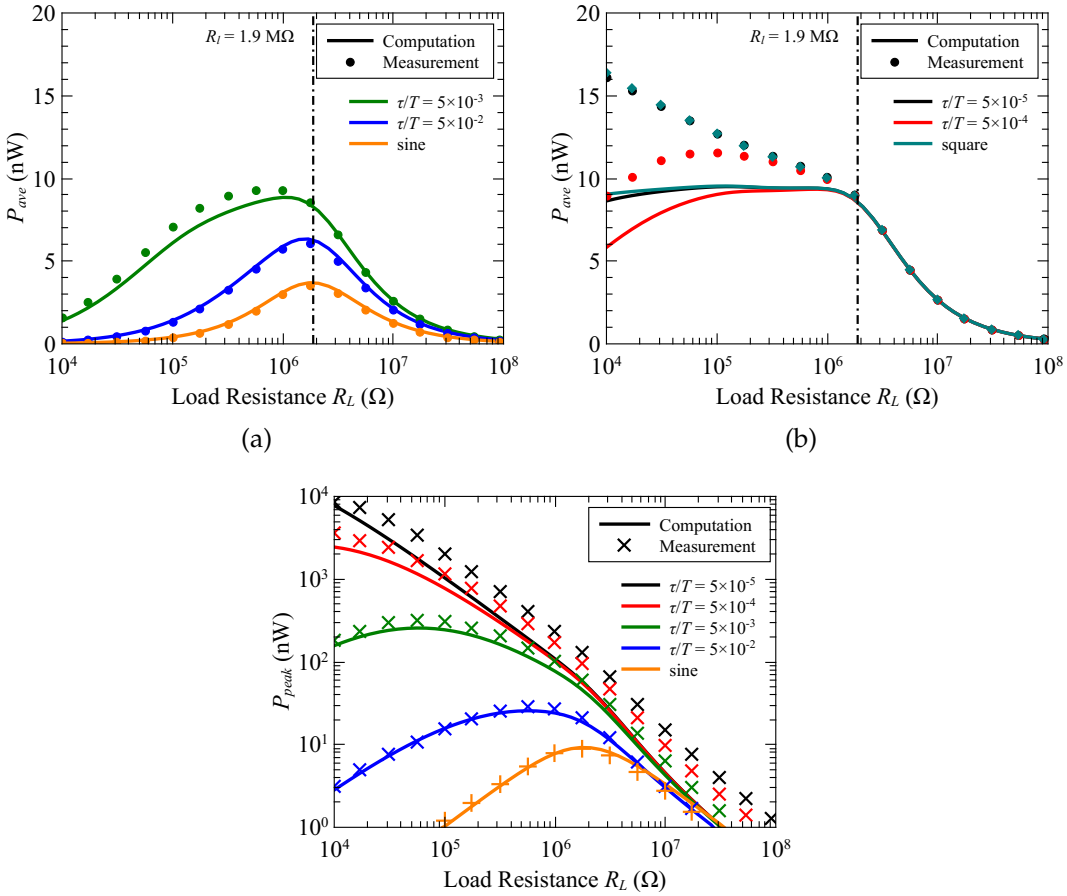

Figure 16: Measured average power (a), (b) and peak power (c) for the PZT buzzer compressed by a NAC2015 actuator, for different values of τ/T. The curves for an exponential signal with $\tau/T = 5 \times 10^{-5}$ and for the square signal are superimposed.

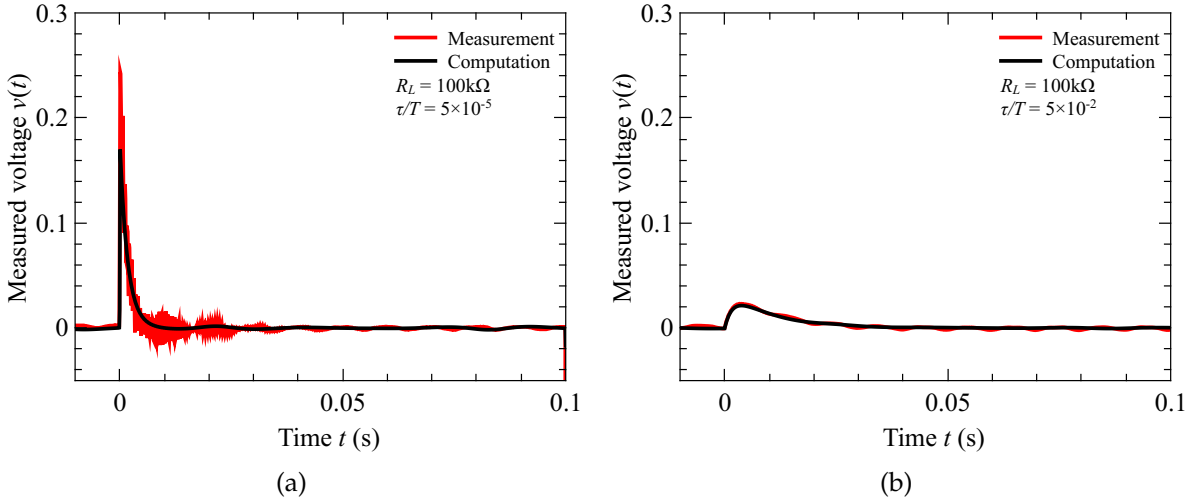

Figure 17: Measured and computed waveform for $R_L = 100\,\text{k}\Omega$, for an exponential signal with $\tau/T = 5 \times 10^{-5}$ (a) and $\tau/T = 5 \times 10^{-2}$ (b).

τ/T decreases and the position of this maximum of power shifts towards small resistance values. The ratio between peak value and average value is 2.5 for the sine waveform; choosing the peak power as a performance metric is still a reasonable approximation in that case with an acceptable overestimation of the available power. For the exponential signal with very low values of τ/T, the peak power is 1000 times higher than the average power, demonstrating that peak instantaneous power value largely overestimates the useful power for very impulsive signals.

5. Conclusion

In this paper, we show that the waveform of the PG open circuit voltage, proportional to the force applied to the PG in quasi-static conditions, largely influences the PGs output power. The study is focused on PG presenting a capacitive internal impedance. Using the Fourier series decomposition, we show that the harmonic content of the PG open circuit voltage strongly influences the harvested power, since the capacitive internal impedance associated with the resistive load enhances the contribution of high frequency harmonics of the signal. This frequency decomposition allows us to highlight that the overall $P(R_L)$ consists of the sum of $P(R_L)$ curves for each harmonic, as a consequence, the optimal load and the shape of the power curve is greatly affected by the harmonic content of the voltage waveform.

The present study also shows that the peak instantaneous power, often referred as a performance metric of PGs, is largely affected by the mechanical excitation waveform, especially for impulsive excitations. Moreover, this study highlights that the peak instantaneous power leads to a large overestimation of the available power when the waveform presents fast transitions. Consequently, for any practical application, the mechanical excitation waveform must be precisely determined in order to correctly estimate the possible harvested power, as well as the optimal load, as these data are necessary to design the rectifying and conversion circuit, dedicated to the targeted electrical load.

Acknowledgement

This project has received funding from the ECSEL JU under grant agreement N°692482. This JU receives support from the European Union's H2020 research and innovation program and France, Netherlands, Denmark, Belgium, Germany, Czek Republic, Spain.

The Authors are also grateful for the supports from Region Centre (MEPS project 2015-2018) and National Research Agency (ANR-14-CE08-0010-01).

References

[1] G. Zhu, A. C. Wang, Y. Liu, Y. Zhou, Z. L. Wang, Functional electrical stimulation by nanogenerator with 58 V output voltage, Nano Letters 12 (6) (2012) 3086–3090. doi:10.1021/nl300972f.

[2] C. Opoku, A. S. Dahiya, F. Cayrel, G. Poulin-Vittrant, D. Alquier, N. Camara, Fabrication of field-effect transistors and functional nanogenerators using hydrothermally grown ZnO nanowires, RSC Adv. 5 (2015) 69925–69931. doi:10.1039/C5RA11450K.

[3] R. Tao, M. Parmar, G. Ardila, P. Oliveira, D. Marques, L. Montès, M. Mouis, Performance of ZnO based piezo-generators under controlled compression, Semiconductor Science and Technology 32 (6) (2017) 064003. doi:10.1088/1361-6641/aa691f.

[4] N. Gogneau, N. Jamond, P. Chrétien, F. Houzé, E. Lefeuvre, M. Tchernycheva, From single III-nitride nanowires to piezoelectric generators: New route for powering nomad electronics, Semiconductor Science and Technology 31 (10) (2016) 103002. doi:10.1088/0268-1242/31/10/103002.

[5] S. Xu, B. J. Hansen, Z. L. Wang, Piezoelectric-nanowire-enabled power source for driving wireless microelectronics, Nature Communications (2010) 93doi:10.1038/ncomms1098.

[6] Y. Hu, Y. Zhang, C. Xu, L. Lin, R. L. Snyder, Z. L. Wang, Self-powered system with wireless data transmission, Nano Letters 11 (6) (2011) 2572–2577. doi:10.1021/nl201505c.

[7] S. Roundy, P. K. Wright, A piezoelectric vibration based generator for wireless electronics, Smart Materials and Structures 13 (5) (2004) 1131.

[8] Z. Lin, J. Chen, X. Li, Z. Zhou, K. Meng, W. Wei, J. Yang, Z. L. Wang, Triboelectric nanogenerator enabled body sensor network for self-powered human heart-rate monitoring, ACS Nano 11 (9) (2017) 8830–8837. doi:10.1021/acsnano.7b02975.

[9] S. Xu, Y. Qin, C. Xu, Y. Wei, R. Yang, Z. L. Wang, Self-powered nanowire devices, Nature Nanotechnology 5 (2010) 366. doi:10.1038/nnano.2010.46.

[10] M. Marzencki, Y. Ammar, S. Basrour, Integrated power harvesting system including a MEMS generator and a power management circuit, Sensors and Actuators A: Physical 145-146 (Supplement C) (2008) 363 – 370. doi:https://doi.org/10.1016/j.sna.2007.10.073.

[11] P. Miribel-Català, J. Colomer-Fararons, J. L. Brinquis, J. López-Sánchez, Self-powered adaptive circuit sampling for a piezoelectric harvester, in: Design of Circuits and Integrated Systems, IEEE, 2014, pp. 1–6. doi:10.1109/DCIS.2014.7035581.

[12] D. Zhu, S. P. Beeby, M. J. Tudor, N. R. Harris, A credit card sized self powered smart sensor node, Sensors and Actuators A: Physical 169 (2) (2011) 317 – 325. doi:https://doi.org/10.1016/j.sna.2011.01.015.

[13] H. Wei, D. Cui, J. Ma, L. Chu, X. Zhao, H. Song, H. Liu, T. Liu, N. Wang, Z. Guo, Energy conversion technologies towards self-powered electrochemical energy storage systems: the state of the art and perspectives, J. Mater. Chem. A 5 (2017) 1873–1894. doi:10.1039/C6TA09726J.

[14] Q. Xu, Y. Qin, Theoretical study of enhancing the piezoelectric nanogenerator's output power by optimizing the external force's shape, APL Materials 5 (7) (2017) 074101. doi:10.1063/1.4975772.

[15] O. Graton, G. Poulin-Vittrant, A. S. Dahiya, N. Camara, L.-P. T. H. Hue, M. Lethiecq, Equivalent circuit model of a nanogenerator based on a piezoelectric nanowire–polymer composite, physica status solidi (RRL) – Rapid Research Letters 7 (10) (2013) 915–918. doi:10.1002/pssr.201308017.

[16] Poulin, Guylaine, Costa, F., Sarraute, E., Minazara, E., Non linear method for the amplification of electrical power delivered by a piezoelectric generator, Eur. Phys. J. Appl. Phys. 33 (2) (2006) 121–132. doi:10.1051/epjap:2006017.

[17] X. Zhou, Q. Xu, S. Bai, Y. Qin, W. Liu, Theoretical study of the $BaTiO_3$ powder's volume ratio's influence on the output of composite piezoelectric nanogenerator, Nanomaterials 7 (6). doi:10.3390/nano7060143.

[18] A. Doria, C. Medè, D. Desideri, A. Maschio, L. Codecasa, F. Moro, On the performance of piezoelectric harvesters loaded by finite width impulses, Mechanical Systems and Signal Processing 100 (2018) 28 – 42. doi:10.1016/j.ymssp.2017.07.030.

[19] M. Renaud, P. Fiorini, C. van Hoof, Optimization of a piezoelectric unimorph for shock and impact energy harvesting, Smart Materials and Structures 16 (4) (2007) 1125. doi:10.1088/0964-1726/16/4/022.

[20] N. Doumit, G. Poulin-Vittrant, A new simulation approach for performance prediction of vertically integrated nanogenerators, Advanced Theory and Simulations 1 (6) (2018) 1800033. doi:10.1002/adts.201800033.

[21] R. Hinchet, S. Lee, G. Ardila, L. Montès, M. Mouis, Z. L. Wang, Performance optimization of vertical nanowire-based piezoelectric nanogenerators, Advanced Functional Materials 24 (7) 971–977. doi:10.1002/adfm.201302157.

[22] R. Tao, G. Ardila, L. Montès, M. Mouis, Modeling of semiconducting piezoelectric nanowires for mechanical energy harvesting and mechanical sensing, Nano Energy 14 (2015) 62 – 76. doi:https://doi.org/10.1016/j.nanoen.2014.11.035.

[23] A. S. Dahiya, F. Morini, S. Boubenia, K. Nadaud, D. Alquier, G. Poulin-Vittrant, Organic/inorganic hybrid stretchable piezoelectric nanogenerators for self-powered wearable electronics, Advanced Materials Technologies (2017) 1700249doi:10.1002/admt.201700249.

[24] G. Zhu, Y. Zhou, S. Wang, R. Yang, Y. Ding, X. Wang, Y. Bando, Z. L. Wang, Synthesis of vertically aligned ultra-long ZnO nanowires on heterogeneous substrates with catalyst at the root, Nanotechnology 23. doi:10.1088/0957-4484/23/5/055604.

[25] X. Chen, S. Xu, N. Yao, Y. Shi, 1.6 V nanogenerator for mechanical energy harvesting using PZT nanofibers, Nano Letters 10 (6) (2010) 2133–2137. doi:10.1021/nl100812k.

[26] R. Yang, Y. Qin, L. Dai, Z. L. Wang, Power generation with laterally packaged piezoelectric fine wires, Nature Nanotechnology 4 (2008) 34.
URL https://doi.org/10.1038/nnano.2008.314

[27] J. Briscoe, N. Jalali, P. Woolliams, M. Stewart, P. M. Weaver, M. Cain, S. Dunn, Measurement techniques for piezoelectric nanogenerators, Energy Environ. Sci. 6 (2013) 3035–3045. doi:10.1039/C3EE41889H.

[28] J. Briscoe, M. Stewart, M. Vopson, M. Cain, P. M. Weaver, S. Dunn, Nanostructured p-n junctions for kinetic-to-electrical energy conversion, Advanced Energy Materials 2 (10) (2012) 1261–1268. doi:10.1002/aenm.201200205.

[29] K. Nadaud, F. Morini, A. S. Dahiya, C. Justeau, S. Boubenia, K. P. Rajeev, D. Alquier, G. Poulin-Vittrant, Double buffer circuit for the characterization of piezoelectric nanogenerators based on ZnO nanowires, Applied Physics Letters 112 (2018) 063903. doi:10.1063/1.5018145.

[30] K. M. Hamdia, H. Ghasemi, X. Zhuang, N. Alajlan, T. Rabczuk, Sensitivity and uncertainty analysis for flexoelectric nanostructures, Computer Methods in Applied Mechanics and Engineering 337 (2018) 95 – 109. doi:https://doi.org/10.1016/j.cma.2018.03.016.

[31] Nac2015.
URL http://www.noliac.com/products/actuators/plate-actuators/show/nac2015/

[32] W. P. Mason, Piezoelectric crystals and their application to ultrasonics, New York, Van Nostrand, 1950.